

# Identification of Acute Myocardial Infarction from Left Ventricular Wall Rupture Using ResNet 18-Deep Active Learning Algorithms



Rajeswari Periyasamy\*<sup>ORCID</sup>, Srinivasan Selvaraj<sup>ORCID</sup>

Department of Computer Science and Engineering, R.M.D. Engineering College, Kavaraipettai 601206, India

Corresponding Author Email: [prw.cse@rmd.ac.in](mailto:prw.cse@rmd.ac.in)

Copyright: ©2024 The authors. This article is published by IETA and is licensed under the CC BY 4.0 license (<http://creativecommons.org/licenses/by/4.0/>).

<https://doi.org/10.18280/ts.410523>

## ABSTRACT

**Received:** 5 September 2023

**Revised:** 3 April 2024

**Accepted:** 12 July 2024

**Available online:** 31 October 2024

### Keywords:

*myocardial infarction, left ventricular wall rupture, left ventricular ejection ratio, deep denoised convolutional neural network (DnCNN), deep active curriculum learning (DACL)*

Acute myocardial infarction (AMI) is a heart muscle ischemia caused by blockage or narrowing of coronary arteries, leading to left ventricular wall rupture (LVWR). Diagnosing AMI is challenging due to improper border and edge enhancement, segmentation, and classification. To address the above-mentioned, a deep denoised convolutional neural network (DnCNN) is applied to enhance the edge and boundary regions of the myocardium. A ResNet 18-based deep active curriculum learning (DACL) model is proposed to classify MI or non-MI patients by left ventricular wall rupture. The model is trained with a few samples to detect MI and dynamically updates the number of samples in the training dataset. The adaptive sampling strategy efficiently classifies myocardial infarction in the HMC-QU dataset, achieving a sensitivity of 98.2%, a specificity of 97.3%, an accuracy of 98.5%, and an AUC of 99.6%.

## 1. INTRODUCTION

According to the World Health Organization, heart disease is the leading cause of death in India, accounting for nearly 54.1% of deaths in 2020. The majority of deaths occur in adults between the ages of 30 and 69, and high blood pressure, poor diabetes control, high cholesterol, and obesity are all causes of heart disease. Heart disease affects both the heart and the arteries. Doctors classify heart disease into several types, including peripheral arterial disease (PAD), cerebrovascular disease (CVD), aortic aneurysm, cardiomyopathy, hypertensive heart disease, heart failure, pulmonary heart disease, and arrhythmias-congenital heart disease, eosinophilic myocarditis [1].

Imaging techniques such as duplex ultrasound, computed tomography angiography (CTA), or magnetic resonance angiography (MRA) of the lower extremities can be used to assess the anatomic location and severity of stenosis in patients with symptomatic PAD who are candidates for revascularization, to restore blood flow in blocked arteries, according to Gerhard-Herman et al. [2]. Patients with symptomatic PAD may also benefit from these imaging modalities. Individual patients are treated with antiplatelet therapy, aspirin and clopidogrel, statin therapy, antihypertensive therapy, oral anticoagulation, and glycemic control. Acute ischemic stroke occurs because of bleeding in the brain. Non-contrast computed tomography (NCCT) and magnetic resonance imaging (MRI) are used to Physicians treat patients with acute ischemic stroke with emergency intravenous injections, emergency endovascular therapy, and stent retrieval.

The aortic root, through the aortic bifurcation, is all

susceptible to aneurysmal disease. Endovascular aneurysm repair with stent grafts has caused a huge paradigm shift in the field of aortic aneurysm surgery over the past three decades [3, 4]. *Cardiomyopathies* are diseases that cause anatomical and functional changes in the heart muscle. Cardiac magnetic resonance imaging can detect cardiomyopathy. Pharmacologic therapies include diuretics, beta-blockers, angiotensin-converting enzyme inhibitors (ACEIs), angiotensin-2 receptor blockers (ARBs), mineralocorticoid antagonists (e.g., spironolactone), ivabradine, and sacubitril/valsartan [5].

Hypertensive heart disease causes structural cardiac changes such as left ventricular hypertrophy (LVH) and left atrial (LA) dilatation, leading to an increased risk of atrial fibrillation (AF) or heart failure (HF) from preserved to reduced ejection fraction (HFpEF) (HFrEF). Detection by cardiac magnetic resonance imaging (MRI) is critical. Recently, researchers have shown that sodium-glucose cotransporter 2 (SGLT2) inhibitors can improve symptoms [6]. Changes in the structure or function of the right ventricle associated with impaired respiratory function define pulmonary heart disease (PHD) [7]. Diuretics are used to treat the excess volume, especially if it is associated with right heart congestion. Long-term oxygen therapy is the cornerstone of PHD treatment. Eosinophilic myocarditis [1] is an inflammatory cardiomyopathy characterized by eosinophilic infiltration of cardiac tissue. A large clinical trial is underway for a drug treatment for eosinophilic myocarditis. There are mainly symptomatic and immunosuppressive therapies available. Myocardial remodelling improved with angiotensin-converting enzyme inhibitors/angiotensin receptor blockers and aldosterone receptor antagonists. Blood pressure medications are used to treat congenital heart disease

(CHD) [8].

## 2. RELATED WORK

A heart attack, called an acute myocardial infarction (AMI), is a potentially fatal condition that occurs when the blood supply is suddenly interrupted, resulting in tissue damage. The diagnosis of myocardial infarction requires evidence of myocardial necrosis in a clinical situation consistent with acute myocardial ischemia. (1) symptoms of myocardial ischemia, (2) new or presumed new significant ST-segment changes or new left bundle branch block, (3) development of pathological Q waves on the electrocardiogram, (4) imaging

evidence of loss of viable myocardium or new regional wall motion abnormality, or (5) identification of an intracoronary thrombus by angiography or autopsy are all symptoms of myocardial infarction. The classification distinguishes between type 1 myocardial infarction, caused by atherosclerotic plaque thrombosis, and type 2 myocardial infarction, caused by an imbalance of myocardial oxygen supply and demand in another acute condition. Sudden myocardial infarctions are percutaneous coronary intervention (type 4) and coronary artery bypass grafting (type 5) [9]. AMI is caused by physical inactivity, alcohol use, smoking, dyslipidemia, diabetes, hypertension, obesity, BMI, stress, gout, age, and periodontal disease [10]. Table 1 shows the state of the art in the detection of myocardial infarction.

**Table 1.** State of the art comparison techniques

Author	Method/Data Used	Cons	Dataset/Metrics
[11]	Shallow neural network ECG signal	Limited ability to capture complex hierarchical patterns	Physikalisch-Technische Bundesanstalt (PTB) Accuracy: 98%
[12]	Multi channel lightweight network(MLNET)/ECG Signal	Fusion of the Complex feature is difficult	Physikalisch-Technische Bundesanstalt (PTB) Accuracy: 96.5%
[13]	CNN-LSTM	Large data required	85.1%
[14]	Encoder -Decoder with CNN SVM	The performance of Encoder and decoder depends on the quantity and quality of the data	HMC-QU Dataset Accuracy 88.92
[15]	Active polynomial+ Echocardiogram	Required specialized knowledge	HMC -QU Dataset Accuracy 87.94%
[16]	Knowledge graph/12 lead ECG signal	Creation of accurate ontology is complex	Physikalisch-Technische Bundesanstalt (PTB) Accuracy: 93.65%
[17]	DenseNet (ECG signal)	Requires more computational resources	Physikalisch-Technische Bundesanstalt(PTB) 95%
[18]	Semantic Segmentation (SegNet)- Cardiac MRI	Misclassification of myocardial infarction due to noise in cardiac MRI	Hospital of Qingdao University Left Ventricle Cardiac MRI dataset 95.5%
[19]	Convolutional Neural Network(CNN)-Cardiac MRI	Difficult in detecting small objects due to low contrast MRI	Delayed Enhancement of MRI dataset 95.53%
[20]	RNN -LSTM (3 lead ECG )	Difficult in capturing long term dependencies	PhysioNet STAFF III-97.4%
[21]	Deep LSTM network (single beat ECG)	Difficult to train	PTB-XL database-77.12%
[22]	Polar Residual Network (echocardiography-short axis view)	Lead to instability and convergence	99.6%
[23]	Inception V3 model(echocardiogram)	Requires large amount of data	PLA general Hospital 99.6%
<b>Advantages over</b>			
<b>Efficient learning by selecting</b>			
<b>informative samples.</b>			
<b>Proposed</b>	<b>ResNet 18 based Deep Active Curriculum learning (DACL) (echocardiogram)</b>	<b>Increasing number of samples gradually improve generalization in unseen data.</b>	<b>HMC-QU</b>
<b>Supports better resource allocation by prioritizing the samples.</b>			

Researchers have used various methods to detect AMI, including electrocardiograms and cardiac MRI. They have used deep learning and machine learning models to detect AMI automatically. However, MRI is expensive and not readily available like other imaging modalities. The variation of the ECG signal depends on the patient's mind. Therefore, to avoid these challenges, echocardiogram images are used to detect MI because echocardiograms provide detailed information about the structure of the heart and wall motion abnormalities. Although echocardiogram images are readily available, left ventricular wall abnormalities are unclear due to ultrasound waves. To address these challenges, researchers used the inception v3 model [23], CNN-LSTM [13], and encoder-decoder CNN [14] models to detect and classify MI. Although the models produced accuracy of 99.6%, 85.1%, and 88.92%, however, the models have some disadvantages, such

as the inception v3 model requires a large amount of annotated data, does not capture spatial and temporal characteristics, and requires more computational resources. CNN-LSTM model captures spatial and temporal features; however, the model needs more data augmentation. The Encoder and Decoder CNN model requires a large amount of data and struggles with class imbalance to capture the fine details from segmented lesions. Hence, to avoid the above-mentioned disadvantages, we have used a transverse dyadic wavelet transform to project the wall abnormalities, and a deep denoised convolutional neural network is used to remove noise from the images. The DACL-ResNet 18 architecture is used to detect AMI. The performance of the proposed model is enhanced by adding selective samples through a deep, active curriculum learning strategy.

## 2.1 Contribution

(1). To extract local and global frequency information from an image, we have used transverse dyadic wavelet transform (TxDyWT) by computing low and high-frequency components at different scales.

(2). To remove noise and protect the corners and edges of the left ventricular wall, we have used a deep denoised convolutional neural network (DnCNN).

(3). To extract the features from a deep denoised image, we have used ResNet 18 architecture, and to improve the performance of the proposed transfer learning ResNet 18 architecture, the deep active curriculum learning model is used to update the training samples dynamically using various sampling techniques, including least significant, entropy, random, and Bayesian active learning by disagreement (BALD).

In this paper, Section 2 describes the state-of-the-art techniques used in the identification of AMI. Section 3

describes the proposed methodology. Section 4 presents the results and discussions. Section 5 presents the conclusion and future work.

## 3. METHODOLOGY

The overall architecture of the proposed deep active curriculum learning model for detecting acute myocardial infarction via left ventricular wall rupture is shown in Figure 1. Echocardiogram images are initially of poor quality. The images are pre-processed with a dyadic wavelet transform and a deep denoised convolutional neural network to improve their quality. The images are labeled as MI or non-MI. The dataset is then divided into training and test sets. Then, we use the ResNet 18 deep active curriculum learning technique to dynamically update the samples to improve the accuracy of our model by evaluating the precision, recall, and accuracy of our proposed method.

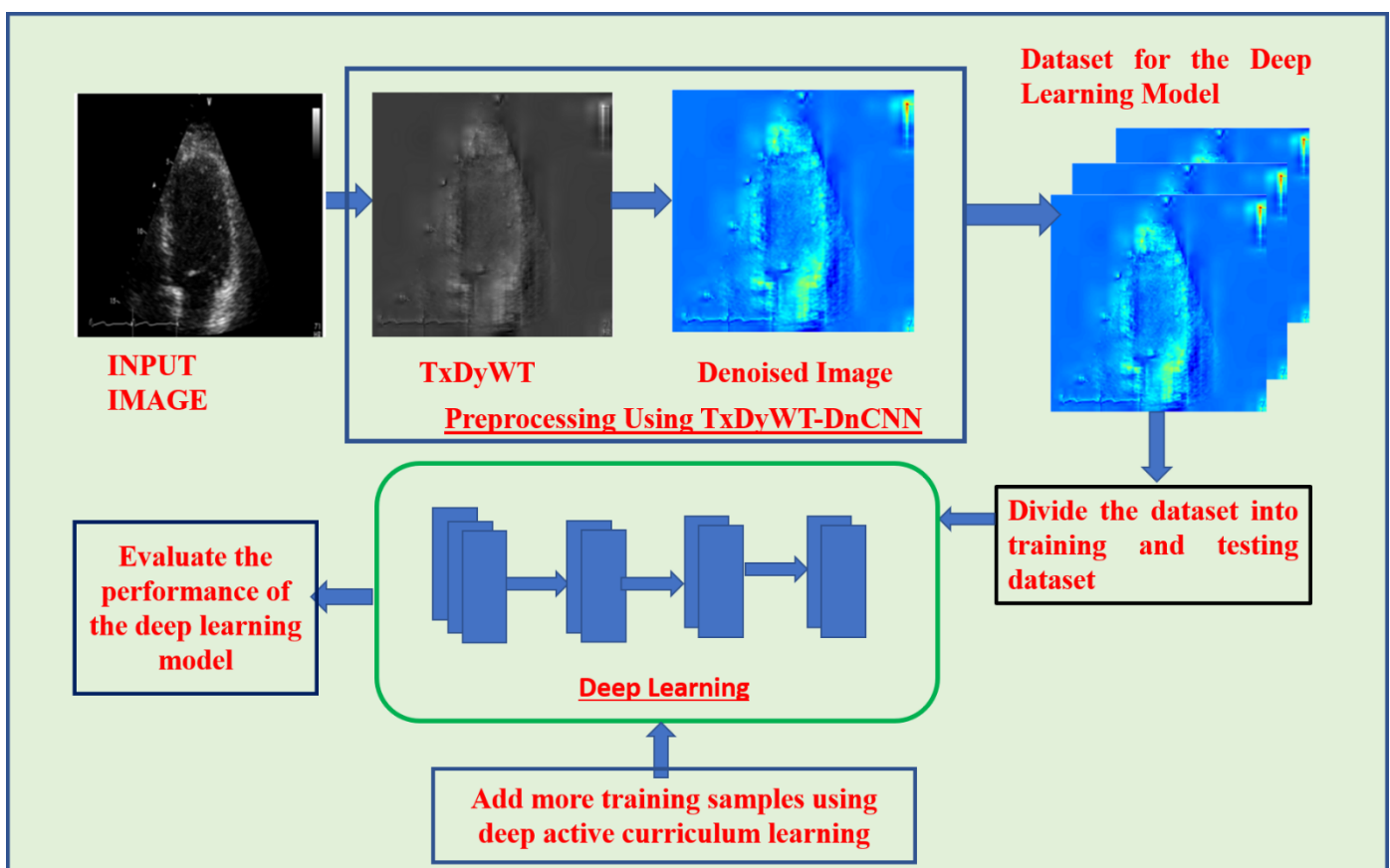


Figure 1. Architecture of ResNet 18-DACL

### 3.1 Image enhancement through TxDyWT-DnCNN

We cannot directly process raw medical images for real-time image processing applications. Because medical images are larger and contain large spatial coordinates of images, the images are in high-dimensional values. There is no standardization of medical image data because different medical images contain different methods such as X-ray, CT scan, MRI, and ultrasound. Each image varies in pixel value, dynamic range, and high resolution. Medical images have complex structures and different patterns, and images are noisy due to different radiation exposures, instruments, and differences in image acquisition. Medical images are gray.

Due to the above characteristics, it is difficult to interpret and analyze medical images. To avoid this problem, the image is pre-processed to improve the image quality. Therefore, we have applied the transverse dyadic wavelet transformation with a deep learning denoised network to improve the visibility and contrast in the analysis of medical images.

#### 3.1.1 Transverse dyadic wavelet transform (TxDyWT)

TxDyWT is a technique for representing images as a collection of wavelets in the time and frequency domains. Wavelets that are referred to as dyadic are those that have been repeatedly translated and expanded. In our work, we improved the segments of different left ventricles using TxDyWT. By

using the five-level Haar wavelet transform, it separates the low-frequency and high-frequency components. From the approximate image, it extracts the details at each level. The discrete Haar wavelet transform is a combination of  $2^n$  and the Haar matrix is represented as in Eq (1):

$$H(n) = \begin{bmatrix} H(n-1) & \otimes [1 \ 1] \\ 2^{\frac{n-1}{2}} I(n-1) & \otimes [1 \ -1] \end{bmatrix} H(0)=1 \quad (1)$$

where,  $H(n) \neq H(n)^T$  for  $n>1$  and  $H(n)$  is a discrete matrix. Haar function and  $I(n)$  is the identity matrix of degree  $2^n$ .  $\otimes$  denotes the product.

The process of obtaining the original image by filtering, adding, and up sampling the inverse wavelet transform of the same wavelet is known as wavelet transform reconstruction. The information is lost due to the same type of inverse wavelet transform. Therefore, the different wavelet transform is used to reconstruct the image to avoid the above problem. Therefore, the different wavelet transforms used for the reconstruction process improves the accuracy, reduces the computational complexity, and lack of information loss results in improved image features during the reconstruction process. Because of the high compression capacity of the Coiflet wavelet, we used it to reconstruct a myocardium of two-chamber echocardiogram, then the image is given to the deep denoised convolutional neural network to remove the noise from the image.

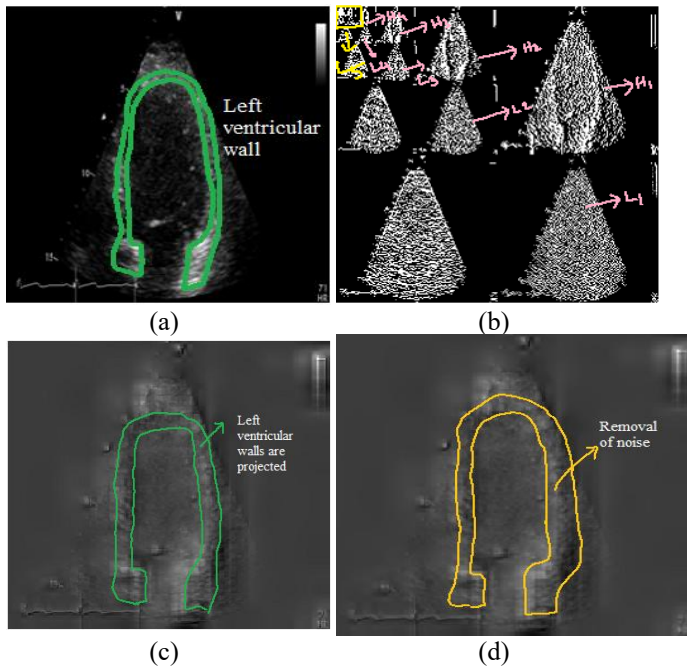


**Figure 2.** Image pre-processing using transverse dyadic wavelet transform and deep denoised convolutional network. (a) Original image (b) Decomposed image (c) Reconstructed image (d) Denoised image

Figure 2 shows the pre-processing of raw echocardiogram images using TxDWT and DnCNN. We cannot directly process raw echocardiogram images because the image quality is poor. Processing medical images with poor quality leads to misclassification of MI. To improve the classification accuracy using ResNet 18 based DACL model, we have pre-processed the 2D myocardial chamber images. The proposed

TxDWT extracts frequency information at different scales, and high frequency components capture the global details and low frequency components capture the local details from the image. Level 5 decomposition effectively captures small variations and abnormalities to effectively capture tissue characteristics and avoid excessive dimensionality, which reduces the computational complexity. Although TxDWT reduces the noise, TxDyWT cannot completely eliminate the noise in echocardiogram images. Therefore, additional DnCNN image denoising techniques are used to remove the noise by improving sharpness and learning complex mapping by preserving the fine details of the echocardiogram image. We have used the input image size as  $224 \times 224$  with 52 layers of deep learning network, the model removes the noise and preserves the fine details of the reconstructed image. Therefore, the model is able to discriminate MI and non-MI segmental view of echocardiogram images effectively.

### 3.2 Deep active curriculum learning (DACL)

Deep learning (DL) and active learning (AL) are subfields of machine learning models. Because of its complicated structure, DL has significant learning capabilities, but it also requires a large number of labeled examples to complete training. The learning process in active curriculum learning is guided by a curriculum, which determines the order and difficulty of the tasks that the learning system should perform. The curriculum is dynamically updated based on the learning system's success in these activities, allowing the system to actively choose which tasks to focus on next and to change the curriculum as it learns. Through the integration of ACL and DL, we enhance efficiency, boost model performance, improve interpretability, handle unbalanced data better, and adapt dynamically.

The Figure 3 shows the architecture of deep active curriculum learning model.

*Algorithm: Least Significant*

*Input: Labeled dataset  $D=\{(x_1,y_1),\dots,(x_n,y_n)\}$ , Unlabeled dataset  $U=\{u_1,\dots,u_m\}$ , initial model  $f_0$*

*Output: Trained model  $f_T$*

(1). Set  $T$ =total number of iterations,  $k=1$ , and initialize the model  $f=f_0$

(2). Define the curriculum order  $c_1,\dots,c_n$  for the labelled dataset  $D$

(3). Define the initial set of query indices  $Q$ =curriculum order  $c_1,\dots,c_N$

(4). while  $k \leq T$  do

*Train the model  $f$  on labelled dataset  $D$  using  $Q$  as training indices*

*Evaluate the model  $f$  on unlabelled dataset  $U$*

*Compute the difficulty scores  $d(u)$  for each unlabelled sample  $u$  in  $U$*

*Compute the expected gradient magnitude for each unlabelled sample  $u$  in  $U$  using  $f$  and  $d(u)$*

*Select the top- $k$  samples with the highest expected gradient magnitude*

*Label the top- $k$  samples and add them to the labelled dataset  $D$*

*Update the curriculum order using the newly labelled samples*

*Set  $Q$  to the new curriculum order*

*Increment  $k$  by 1*

*end while*

*Return the final model  $f_T$*

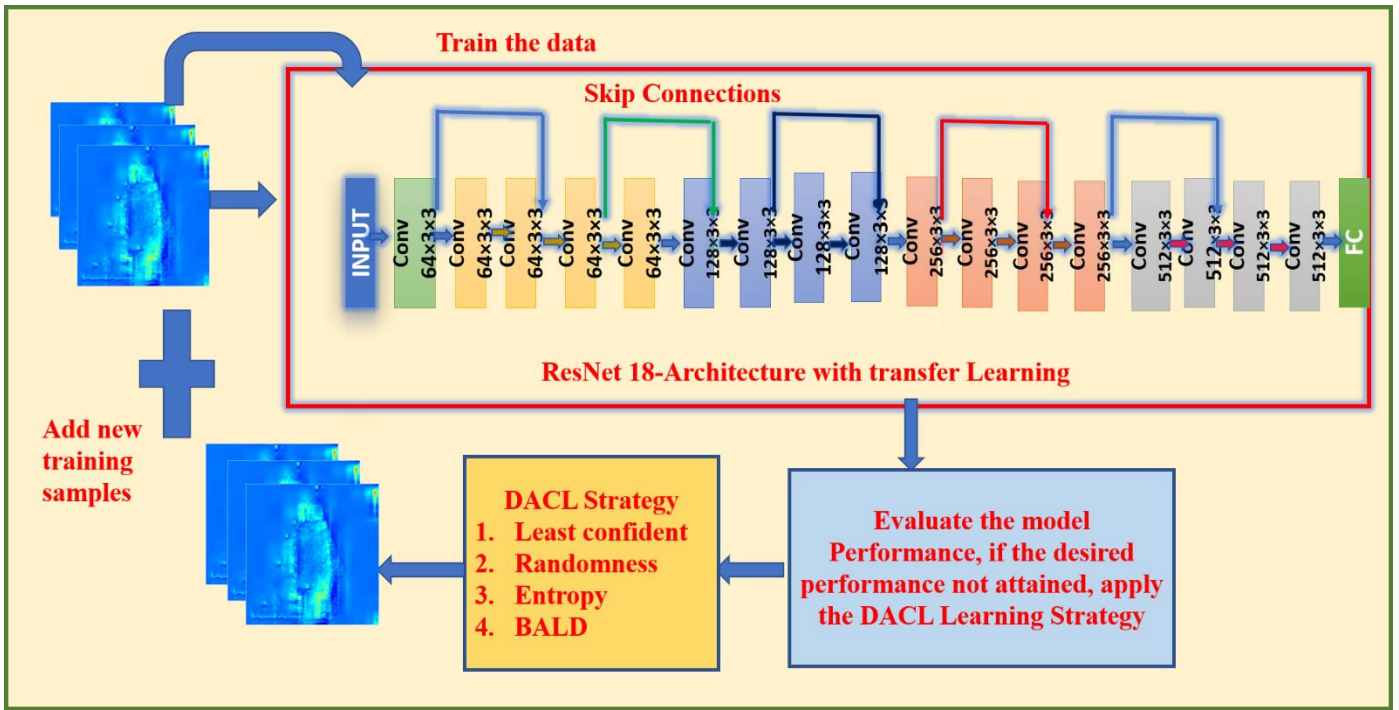


Figure 3. Deep active curriculum learning with ResNet 18 architecture

### 3.2.1 Entropy

Uncertainty Sampling is a machine learning technique for selecting informative samples for human labelling. The purpose of this method is to choose the samples with the least confident predictions. The uncertainty in a distribution is quantified by its entropy. The entropy is calculated using Eq. (2):

$$H(p) = - \sum p(x) \log(p(x)) \quad (2)$$

where,  $p(x)$  is the probability that the model predicts class  $x$  for the given sample. The entropy value ranges from 0 to  $\log(C)$ , where  $C$  is the number of classes in the classification problem. A lower entropy value indicates that the model is more confident in its prediction for the sample. The least confident sampling method selects the samples with the lowest maximum probability. Mathematically, for a given sample  $x$ , the least confident score is calculated as in Eq. (3):

$$LC(x) = \max(p(x)) \quad (3)$$

where,  $p(x)$  is the probability distribution over the classes predicted by the model for the sample  $x$ . The sample with the lowest LC score is the one for which the model is least confident in its prediction.

*Algorithm: Entropy*

*Input:*

- *model: a trained machine learning model*
- *data: a set of unlabeled data points*
- *k: the number of data points to select*

*Output:*

- *A set of k selected data points*
- 1) *Initialize an empty set called selected.*
- 2) *For i=1 to k:*
  - a. *Calculate the model's predicted probabilities for each data point in data.*

*b. Sort the probabilities in descending order.*

*c. Select the data point with the lowest probability and add it to the selected set.*

*d. Remove the selected data point from the data set.*

3) *Return the set of selected data points.*

### 3.2.2 Bayesian active learning by disagreement

Bayesian Active Learning by Disagreement (BALD) is an uncertainty sampling method commonly used in machine learning for model training and testing. BALD is based on Bayesian inference and aims to select the data points that are most informative for the model.

The mathematical expression for BALD is given in Eq. (4):

$$BALD(x) = H(y|x) - E[H(y|x, D)] \quad (4)$$

where,  $H[y|x]$  is the entropy of the model's output distribution for input  $x$ , and  $E[ H[y|x, D] ]$  is the expected entropy of the output distribution if data  $D$  (the training set) were augmented with  $x$ . The BALD measures the difference between the entropy of the model's predictions for  $x$  and the expected entropy of the predictions if  $x$  were added to the training set.

*Algorithm: BALD*

*Input:*

- *model: a trained machine learning model*
- *data: a set of unlabeled data points*
- *k: the number of data points to select*
- *n: the number of Monte Carlo simulations to run*

*Output:*

- *A set of k selected data points*

1) *Initialize an empty set called selected.*

2) *For i = 1 to k:*

a. *For each data point in data, run n Monte Carlo simulations:*

i. *Sample a set of model parameters from the posterior distribution.*

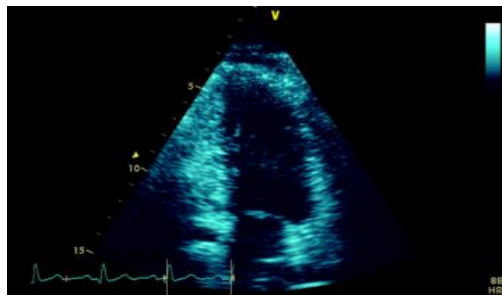
- ii. Use the sampled parameters to generate a prediction for the data point.
  - iii. Record the predicted class probabilities.
- b. For each data point in data, calculate the expected entropy:
    - i. Calculate the entropy of the average predicted class probabilities across the  $n$  simulations.
    - ii. Subtract the average entropy of the predicted class probabilities across the  $n$  simulations for each individual simulation.
    - c. Select the data point with the highest expected entropy and add it to the selected set.
    - d. Remove the selected data point from the data set.
  - 3). Return the set of selected data points.

## 4. RESULTS AND DISCUSSIONS

### 4.1 HMC-QU dataset

**Table 2.** Statistics of 2 chamber view of myocardium

Myocardial Segments	MI Patients	NonMI Patients
Segment 4	29	101
Segment 10	29	101
Segment 15	53	77
Segment 13	47	93
Segment 7	40	90
Segment 1	40	90
Segment 4,10	58	202
Segment 4,15	82	178
Segment 4,13	76	194
Segment 4,7	69	191
Segment 1,4	69	191
Segment 10,15	82	178
Segment 10,7	69	191
Segment 10,1	69	191
Segment 15,13	100	170
Segment 15,7	93	167
Segment 13,1	87	183
All Segments	10	62



2-Chamber View

**Figure 4.** Sample images from dataset

Apical 4-chamber and apical 2-chamber 2D echocardiogram images from 2018 and 2019 make up the HMC-QU benchmark dataset [24]. Hamad Medical Corporation (HMC), in collaboration with the University of Tampere and Qatar University, created the dataset. The collection includes more than 10,000 echoes and more than 800 hospitalized patients with acute ST-elevation MI. Ground-truth names are provided for each cardiac segment. 130 A2C-view echocardiograms and 162 A4C-view echocardiograms in the dataset. The 93 MI patients (all acute, first-time MI patients) and 69 non-MI participants are the owners of the

A4C view recordings. The A2C view 2D echocardiogram recordings belong to 62 non-MI participants and 68 MI patients. The dataset contains ground truth labeling where MI is indicated as 0 and 1 indicates non-MI patients. The spatial resolution of the echocardiogram images is varied from  $422 \times 636$  to  $768 \times 1024$  pixels at 25 frames per second. Table 2 shows the statistics of the 2-chamber segmental view of MI and Non MI patients.

The Figure 4 shows the sample images from the dataset.

### 4.2 Experimental set up

The proposed model is evaluated in 80% of training set and 20% of test set with ResNet 18 DACL model. The echocardiogram images are preprocessed because of noise and ultrasound waves using TxDyWT-DnCNN. Hence, the preprocessed images fed into ResNet 18 architecting and training process is done through deep active curriculum learning techniques. Table 3 shows the model architecture and training parameters.

**Table 3.** Model architecture and training parameter

Model Architecture	ResNet 18 Architecture
Preprocessing	Images are resized with [224×224]
Layers added	Classification layer is added according to output class as 2
Optimizer	Stochastic Gradient with momentum
Number of epochs	10
Validation	Validation is performed for every 50 iterations
Frequency	0.01
Learning rate	0.01

#### 4.2.1 Evaluation metrics

The evaluation metrics are shown in Eqs. (5)-(11).

True Positive(TP): Number of patients correctly classified as AMI.

True Negative(TN): Number of patients correctly classified as not having AMI.

False Positive(FP): Number of patients incorrectly classified as having AMI.

False Negative(FN)=Number of patients incorrectly classified as not having AMI.

$$Precision = TP / (TP + FP) \quad (5)$$

$$Recall = TP / (TP + FN) \quad (6)$$

$$F1 - Score = 2 * (precision * recall) / (precision + recall) \quad (7)$$

$$Accuracy = (TP + TN) / (TP + TN + FP + FN) \quad (8)$$

$$Sensitivity = TP / (TP + FN) \quad (9)$$

$$Specificity = \frac{TN}{FP + TN} \quad (10)$$

$$AUC = True Positive Rate / False Positive Rate \quad (11)$$

### 4.3 Preprocessing technique

Speckle noise, Gaussian noise, shadowing and attenuation, and ringing noise all affect ultrasound imaging. Speckle noise creates small circles in the image. The clarity of an image is

affected by Gaussian noise. The image becomes darker and less clear due to attenuation and shadows. Ringing is caused by a series of oscillations around the edges of the image. Ringing affects the image structure. The reconstructed dyadic wavelet transformed image is passed through a deep denoised convolutional neural network to reduce noise. Peak Signal to

Noise Ratio (PSNR), Structural Similarity Index (SSIM), Mean Square Error (MSE), and Blind/Reference less Picture Spatial Quality Evaluator (BRISQUE) [25] are used to quantify the quality of the image metrics. The Figure 5 shows the original, dyadic wavelet image, and the deep denoised image. Figure 6 shows the image quality metrics.

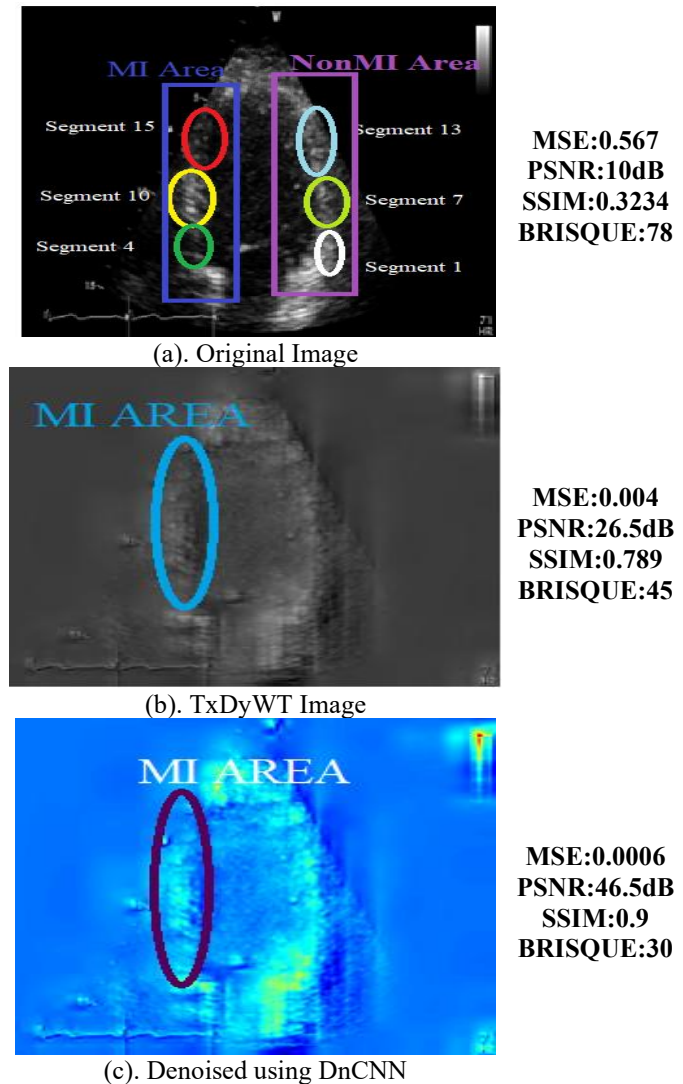


Figure 5. (a). Original image (b). Dyadic wavelet image (c). Deep denoised image

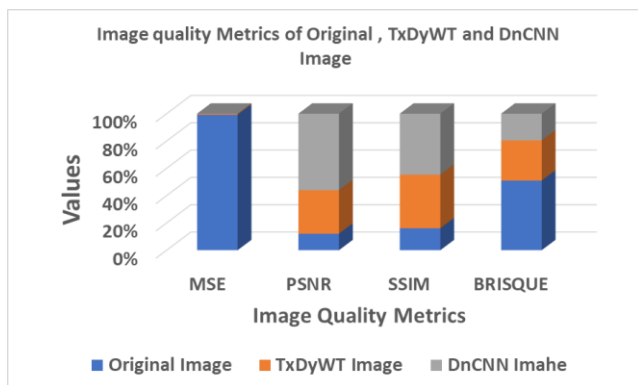


Figure 6. Image quality metrics

The difference between the original and the denoised image is measured by the peak signal-to-noise ratio (PSNR). PSNR is measured in dB (decibels). A higher PSNR value indicates a higher quality image with less noise.

$$PSNR = 10 * \log_{10}\left(\frac{MAX^2}{MSE}\right) \quad (12)$$

In Eq. (5), MAX is the maximum possible pixel value in the image. MSE is the mean square error.

Structure Similarity Index measures the quality between two images. The values are in the range between [0, 1]. 1- means that two images are similar.

$$SSIM(x, y) = [l(x, y) * c(x, y) * s(x, y)] \quad (13)$$

In Eq. (13),  $l(x, y)$  represents luminance,  $c(x, y)$  represents contrast, and  $s(x, y)$  represents structure.

Mean Square Error measures the error between the original image and the denoised image.

$$MSE = \frac{1}{N} \sum_{i=1}^N x_i - y_i^2 \quad (14)$$

In Eq. (14),  $N$  represents the total number of pixels in an image,  $x_i$  is a pixel in an original image, and  $y_i$  represents a pixel in the denoised image. A lower MSE value represents a good quality image.

Blind/Reference less Image Spatial Quality Evaluator (BRISQUE) measures the image naturalness pixel by pixel on the denoised image. The BRISQUE score is between [0-100]. Lower score value produces better quality of an image.

The metrics for the original echocardiogram and the denoised image is shown in Figure 6. Echocardiogram images are noisier and have less contrast. We used the DnCNN network to improve the image quality. The image quality was greatly improved by the denoising process, which led to an increase in contrast and a decrease in noise level. With this advancement, heart disease can be more accurately diagnosed and treated. MSE, PSNR, SSIM and BRISQUE are metrics used to determine the quality of an image. MSE values for echocardiogram images should be less than 10, PSNR values between 25 and 40 dB, SSIM values between 0.5 and 0.9, and BRISQUE values between 10 and 60. The DnCNN network performed well in each of these metrics, which provide quantitative assessments of image quality. The success of this method suggests that denoising techniques based on deep learning is useful in medical imaging applications. As a result, the DnCNN network improves the image quality of echocardiograms.

#### 4.4 Least significant uncertainty strategy

The least significant sampling strategy is used to select crucial data samples for training a deep learning network. This method can reduce the number of training samples required, resulting in faster and more efficient model development. Active learning and data augmentation techniques can significantly reduce the amount of data required while maintaining or improving model accuracy. Active Curriculum Learning uses a small sample size at each stage by selecting the least significant samples. The trained network selects samples until it achieves the best performance. The architecture of ResNet18 is modified by increasing the weight and bias of the fully connected FC1000 layer. A new output layer for classification is added to the existing ResNet18 architecture. After 14 trials, the least significant sampling strategy achieves the highest accuracy. Figure 7 shows the training and validation accuracy of ResNet 18 DACL.

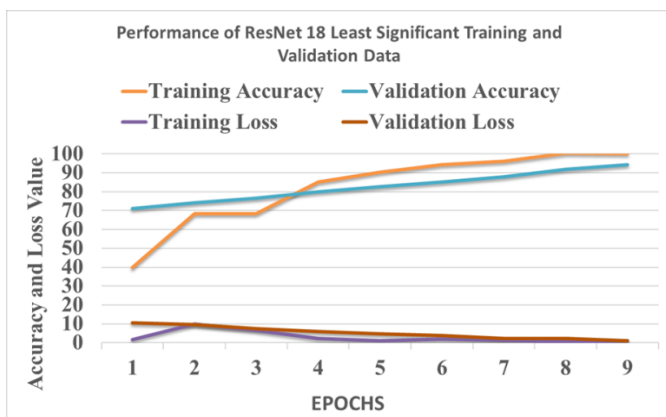


Figure 7. Training and validation loss curve of ResNet 18 DACL

#### 4.5 Uncertainty sampling using entropy

The study utilised entropy-based deep active curriculum learning to collect uncertainty examples from a dataset, enhancing the model's performance and reducing training time compared to traditional methods. The initial training set consisted of 50 samples, and the ResNet18 architecture model was trained with these samples. Entropy was calculated for each probability class, with higher entropy indicating higher uncertainty and lower entropy indicating higher confidence in predictions. The model was fine-tuned using the updated training set, resulting in improved accuracy on the test set. The model added 100 samples for cross-validation, and the process was repeated until the highest recognition accuracy was achieved. The study provides a detailed analysis of the training and testing losses and accuracy of each iteration (Figure 8).

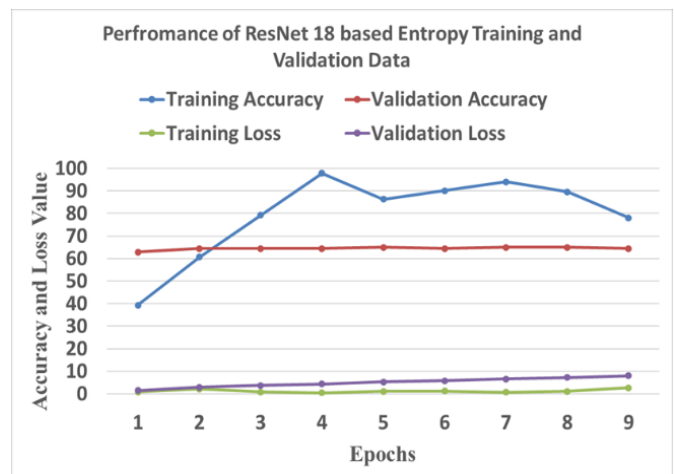


Figure 8. Deep active curriculum learning using entropy method

#### 4.6 Uncertainty sampling using random

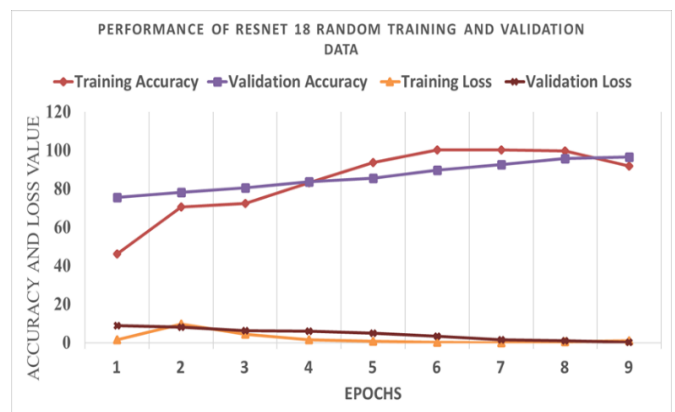


Figure 9. Training and validation accuracy and loss curve of ResNet 18 Random DACL

The random sampling method was used to select samples from an unlabelled sample, ensuring equal chances and reducing bias. This method allowed for statistical inferences about the larger population from which the samples were drawn. The model was initially trained with small, labelled samples to improve its accuracy in predicting outcomes. As the model became more sophisticated, random sampling was used to collect larger, unlabelled samples for further training

and testing. This approach helped refine the model's predictions and increase its effectiveness in real-world applications. However, the random method does not select informative samples, so active learning techniques can be used to select the most informative samples for labelling, reducing the amount of labelled data needed for high accuracy in the model's predictions (Figure 9).

#### 4.7 Uncertainty sampling using BALD

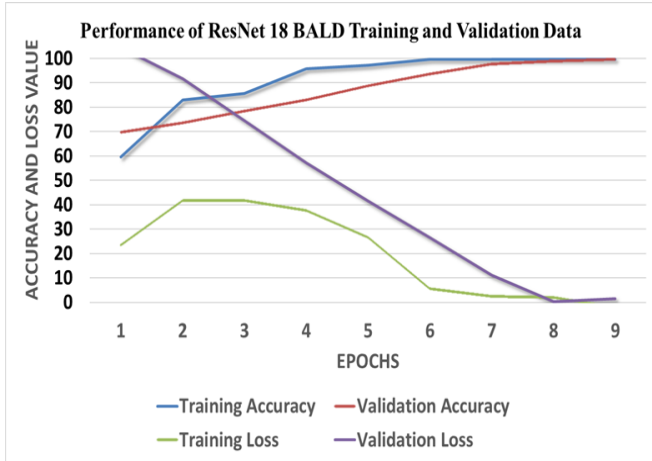


Figure 10. Training, testing accuracy and loss

By computing Bayesian probabilistic inferences, Bayesian active learning by disagreement was used to select the samples. This method makes it possible to efficiently select informative samples for labeling in a classification task. To improve the overall accuracy of the model, the algorithm selects the most uncertain or disagreeing samples among the classifiers. We compute the disagreement using a joint entropy probability distribution. This method is particularly useful when labeling all samples is impractical due to time or cost constraints. The algorithm can achieve high accuracy with fewer labeled examples by prioritizing the most informative samples for

labeling. The Figure 10 shows the training, testing loss, and accuracy of BALD.

#### 4.8 Comparison with state-of-the-art techniques

The Table 4 shows the myocardial infarction detection using CNN-LSTM, Encoder-Decoder CNN+SVM, Inception V3 and proposed model. Among all the methods, the proposed model provides high sensitivity, specificity, accuracy and area under the curve. CNN-LSTM, Inception V3, and Encoder-Decoder CNN+SVM models require high computational power due to the complexity of architecture, lack of interpretability in clinical decision making, needs large amount of labeled data, however, in medical domain large amount of data is challenging due to privacy and imbalance issues, lead to reduced generalization in unseen data, deployment of deep learning model in clinical environment is difficult due to model size, inference speed and integration of existing healthcare system. Therefore, these limitations are solved by our proposed model. The proposed model adds the data slowly by sampling strategy, more interpretable, and computationally efficient and robust for myocardial infarction.

The Figure 11 shows the integration of DACL into the clinical environment. The proposed DACL model plays an important role in accurate detection of myocardial infarction. Echocardiogram has several challenges such as poor image quality due to ultrasound waves, limited visualization in regional wall motion abnormalities, interoperated variability, difficult in diagnosing small infarcts, and temporal resolution of an image. These challenges lead to false diagnosis of accurate detection of myocardial infarction. Therefore, to accurately detect myocardial infarction, artificial intelligence techniques are integrated into picture archiving communication system (PACS). Therefore, our proposed TxDyWT-DnCNN-ResNet 18 DACL model improves the quality of an image and enhances the left ventricular wall to detect infarcted segment in the left ventricle at an early stage. Earlier detection of myocardial infarction increases the survival rate of patients.

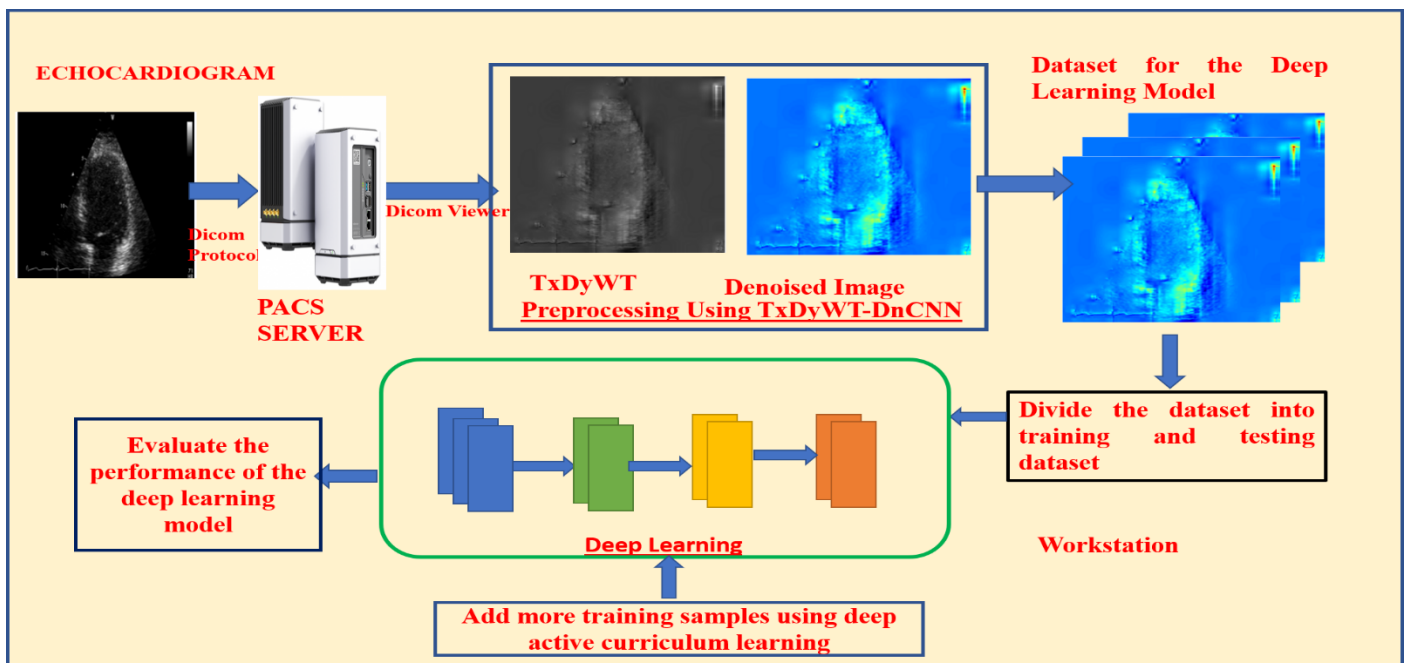


Figure 11. Integration of DACL to clinical environment

**Table 4.** Comparison of state-of-the-art techniques

Author	Sensitivity	Specificity	Accuracy	AUC
[13]	83.8	86.4	85.1	87
[14]	83.09	74.03	80.24	82.2
[15]	96.2	95.3	96.59	98.52
Proposed TxDyWT+DnCNN+ResNet 18 DACL	98.2	97.3	98.5	99.6

## 5. CONCLUSIONS

The difficulties of early detection of acute myocardial infarction are addressed in the conclusion of this study. Traditionally, left ventricular ejection fraction, blood tests, and ECG signal analysis are used to detect AMI. However, these methods have some drawbacks, such as the temporal variation of the ECG signal in ST segment changes and the need for 12-lead ECG signals to detect AMI instead of a single ECG signal. The diagnosis of AMI took longer with the troponin blood markers; this delay affects how quickly the diagnosis is made. It's also important to remember that interpreting ECG signals requires expertise and is susceptible to human error. To detect and treat AMI, it is important to combine multiple diagnostic tools and seek medical attention as soon as possible. Changes in myocardial function may not be detected by LVEF, which instead measures blood flow to the left ventricle. To avoid these problems, we have used echocardiogram image analysis to detect AMI. This technique provides a more accurate assessment of myocardial function and has the ability to detect changes in the structure and function of the heart that may not be apparent with other diagnostic tests. In addition, AMI can be effectively diagnosed and treated early to improve patient outcomes and reduce the risk of complications. With a Left ventricular wall rupture and a short-axis view of the myocardium, a number of deep learning algorithms can detect AMI. However, a larger number of images must be used to train these models. These methods require more time to find AMI. It takes a long time to complete. In order to detect AMI with a small data set, our proposed deep active curriculum learning model uses a sampling strategy to learn the training set. In the future, we'll add actual clinical images to our model to improve it.

## REFERENCES

- [1] Zhong, Z., Yang, Z., Peng, Y., Wang, L., Yuan, X. (2021). Diagnosis and treatment of eosinophilic myocarditis. *Journal of Translational Autoimmunity*, 4: 100118. <https://doi.org/10.1016/j.jtauto.2021.100118>
- [2] Gerhard-Herman, M.D., Gornik, H.L., Barrett, C., Barshes, N.R., Corriere, M.A., Drachman, D.E., Fleisher, L.A., Fowkes, F.G.R., Hamburg, N.M., Kinlay, S., Lookstein, R., Misra, S., Mureebe, L., Olin, J.W., Patel, R.A.G., Regensteiner, J.G., Schanzer, A., Shishehbor, M.H., Stewart, K.J., Treat-Jacobson, D., Walsh, M.E. (2017). AHA/ACC guideline on the management of patients with lower extremity peripheral artery disease: A report of the American college of cardiology/American Heart Association Task Force on Clinical Practice Guidelines. *Circulation*, 135(12): e726-e779. <https://doi.org/10.1161/CIR.0000000000000471>
- [3] Powers, W.J., Rabinstein, A.A., Ackerson, T., Adeoye, O.M., Bambakidis, N.C., Becker, K., Biller, J., Brown, M., Demaerschalk, B.M., Hoh, B., Jauch, E.C., Kidwell, C.S., Leslie-Mazwi, T.M., Ovbiagele, B., Scott, P.A., Sheth, K.N., Southerland, A.M., Summers, D.V., Tirschwell, D.L., American Heart Association Stroke Council. (2019). Guidelines for the early management of patients with acute ischemic stroke: 2019 update to the 2018 guidelines for the early management of acute ischemic stroke: A guideline for healthcare professionals from the American Heart Association/American Stroke Association. *Stroke*, 50(12): e344-e418. <https://doi.org/10.1161/STR.0000000000000211>
- [4] Swerdlow, N.J., Wu, W.W., Schermerhorn, M.L. (2019). Open and endovascular management of aortic aneurysms. *Circulation Research*, 124(4): 647-661. <https://doi.org/10.1161/CIRCRESAHA.118.313186>
- [5] Enzan, N., Matsushima, S., Ide, T., Tohyama, T., Funakoshi, K., Higo, T., Tsutsui, H. (2022). The use of angiotensin II receptor blocker is associated with greater recovery of cardiac function than angiotensin-converting enzyme inhibitor in dilated cardiomyopathy. *ESC Heart Failure*, 9(2): 1175-1185. <https://doi.org/10.1002/ehf2.13790>
- [6] Vischer, A.S., Burkard, T. (2022). Hypertensive heart disease-From pathophysiology to therapeutical challenges. *Journal of Clinical Medicine*, 11(16): 4640. <https://doi.org/10.3390/jcm11164640>
- [7] Forfia, P.R., Vaidya, A., Wiegers, S.E. (2013). Pulmonary heart disease: The heart-lung interaction and its impact on patient phenotypes. *Pulmonary Circulation*, 3(1): 5-19. <https://doi.org/10.4103/2045-8932.109910>
- [8] Stout, K.K., Daniels, C.J., Aboulhosn, J.A., Bozkurt, B., Broberg, C.S., Colman, J.M., Crumb, S.R., Dearani, J.A., Fuller, S., Gurvitz, M., Khairy, P., Landzberg, M.J., Saidi, A., Valente, A.M., Van Hare, G.F. (2019). 2018 AHA/ACC guideline for the management of adults with congenital heart disease: A report of the American college of cardiology/American heart association task force on clinical practice guidelines. *Circulation*, 139(14): e698-e800. <https://doi.org/10.1161/CIR.0000000000000603>
- [9] Chapman, A.R., Adamson, P.D., Mills, N.L. (2017). Assessment and classification of patients with myocardial injury and infarction in clinical practice. *Heart*, 103(1): 10-18. <https://doi.org/10.1136/heartjnl-2016-309530>
- [10] Rathore, V., Singh, N., Mahat, R.K., Kocak, M.Z., Fidan, K., Ayazoglu, T.A. (2018). Risk factors for acute myocardial infarction: A review. *Ejmi*, 2(1): 1-7. <https://doi.org/10.14744/ejmi.2018.76486>
- [11] Jafarian, K., Vahdat, V., Salehi, S., Mobin, M. (2020). Automating detection and localization of myocardial infarction using shallow and end-to-end deep neural networks. *Applied Soft Computing*, 93: 106383. <https://doi.org/10.1016/j.asoc.2020.106383>
- [12] Cao, Y., Wei, T., Zhang, B., Lin, N., Rodrigues, J.J., Li, J., Zhang, D. (2021). ML-Net: Multi-channel lightweight network for detecting myocardial infarction. *IEEE*

- Journal of Biomedical and Health Informatics, 25(10): 3721-3731. <https://doi.org/10.1109/JBHI.2021.3060433>
- [13] Muraki, R., Teramoto, A., Sugimoto, K., Sugimoto, K., Yamada, A., Watanabe, E. (2022). Automated detection scheme for acute myocardial infarction using convolutional neural network and long short-term memory. *PloS One*, 17(2): e0264002. <https://doi.org/10.1371/journal.pone.0264002>
- [14] Degerli, A., Zabihi, M., Kiranyaz, S., Hamid, T., Mazhar, R., Hamila, R., Gabbouj, M. (2021). Early detection of myocardial infarction in low-quality echocardiography. *IEEE Access*, 9: 34442-34453. <https://doi.org/10.1109/ACCESS.2021.3059595>
- [15] Kiranyaz, S., Degerli, A., Hamid, T., Mazhar, R., Ahmed, R.E.F., Abouhasera, R., Zabihi, M., Malik, J., Hamila, R., Gabbouj, M. (2020). Left ventricular wall motion estimation by active polynomials for acute myocardial infarction detection. *IEEE Access*, 8: 210301-210317. <https://doi.org/10.1109/ACCESS.2020.3038743>
- [16] Han, C., Pan, S., Que, W., Wang, Z., Zhai, Y., Shi, L. (2022). Automated localization and severity period prediction of myocardial infarction with clinical interpretability based on deep learning and knowledge graph. *Expert Systems with Applications*, 209: 118398. <https://doi.org/10.1016/j.eswa.2022.118398>
- [17] Jahmunah, V., Ng, E.Y., Tan, R.S., Oh, S.L., Acharya, U.R. (2022). Explainable detection of myocardial infarction using deep learning models with Grad-CAM technique on ECG signals. *Computers in Biology and Medicine*, 146: 105550. <https://doi.org/10.1016/j.compbiomed.2022.105550>
- [18] Yan, Z., Su, Y., Sun, H., Yu, H., Ma, W., Chi, H., Cao, H., Chang, Q. (2022). SegNet-based left ventricular MRI segmentation for the diagnosis of cardiac hypertrophy and myocardial infarction. *Computer Methods and Programs in Biomedicine*, 227: 107197. <https://doi.org/10.1016/j.cmpb.2022.107197>
- [19] Chen, Z., Lalande, A., Salomon, M., Decourselle, T., Pommier, T., Qayyum, A., Shi, J., Perrot, G., Couturier, R. (2022). Automatic deep learning-based myocardial infarction segmentation from delayed enhancement MRI. *Computerized Medical Imaging and Graphics*, 95: 102014. <https://doi.org/10.1016/j.compmedimag.2021.102014>
- [20] Hernandez, A.A., Bonizzi, P., Peeters, R., Karel, J. (2023). Continuous monitoring of acute myocardial infarction with a 3-Lead ECG system. *Biomedical Signal Processing and Control*, 79: 104041. <https://doi.org/10.1016/j.bspc.2022.104041>
- [21] Martin, H., Morar, U., Izquierdo, W., Cabrerizo, M., Cabrera, A., Adjouadi, M. (2021). Real-time frequency-independent single-Lead and single-beat myocardial infarction detection. *Artificial Intelligence in Medicine*, 121: 102179. <https://doi.org/10.1016/j.artmed.2021.102179>
- [22] Guo, Y., Du, G.Q., Shen, W.Q., Du, C., He, P.N., Siuly, S. (2021). Automatic myocardial infarction detection in contrast echocardiography based on polar residual network. *Computer Methods and Programs in Biomedicine*, 198: 105791. <https://doi.org/10.1016/j.cmpb.2020.105791>
- [23] Liu, B., Chang, H., Yang, D., Yang, F., Wang, Q., Deng, Y., Li, L., Lv, W., Zhang, B., Yu, L., Burkhoff, D., He, K. (2023). A deep learning framework assisted echocardiography with diagnosis, lesion localization, phenogrouping heterogeneous disease, and anomaly detection. *Scientific Reports*, 13(1): 3. <https://doi.org/10.1038/s41598-022-27211-w>
- [24] HMC-QU dataset: HMC-QU Dataset | Kaggle: HMC-QU Dataset. [kaggle.com](https://www.kaggle.com/datasets/hmc-quad/hmc-qu-dataset), accessed on May 24, 2023.
- [25] Haque, S., Eberhart, Z., Bansal, A., McMillan, C. (2022). Semantic similarity metrics for evaluating source code summarization. In *Proceedings of the 30th IEEE/ACM International Conference on Program Comprehension*, pp. 36-47. <https://doi.org/10.1145/3524610.3527909>